

# C-axis charge dynamics of BaFe<sub>2</sub>As<sub>2</sub>

Z. G. Chen, T. Dong, R. H. Ruan, B. F. Hu, B. Cheng, W. Z. Hu, P. Zheng, Z. Fang, X. Dai, and N. L. Wang  
*Beijing National Laboratory for Condensed Matter Physics,  
Institute of Physics, Chinese Academy of Sciences, Beijing 100190, China*

We present the c-axis optical reflectance measurement on single crystals of BaFe<sub>2</sub>As<sub>2</sub>. Comparing with the ab-plane optical response, we find a small ratio of anisotropy for free carrier contributions. Most significantly, the work revealed a clear difference in optical conductivity for  $\mathbf{E}\parallel\text{ab-plane}$  and  $\mathbf{E}\parallel\text{c-axis}$  in the SDW state. The very pronounced energy gap structure seen at a higher energy scale for  $\mathbf{E}\parallel\text{ab-plane}$  is almost invisible for  $\mathbf{E}\parallel\text{c-axis}$ , whereas the smaller energy gap could be seen in both polarizations. We propose a novel picture for the band structure evolution across the SDW transition and suggest different driving mechanisms for the formation of the two energy gaps.

PACS numbers: 74.25.Gz, 74.70.Xa, 75.30.Fv

For quasi-two dimensional layered materials, there appears striking difference in charge transport between ab-plane and along the c-axis. A typical example is the high-Tc cuprates in the underdoped or optimally doped regions where the CuO<sub>2</sub>-planes appear to be almost decoupled in the normal state. The in-plane charge transport is metallic, whereas the c-axis is insulator-like.[1] The fundamental difference leads to the suggestion that the charge carriers are confined within the CuO<sub>2</sub>-planes. This was taken as a standing ground for some theoretical proposals, for example the exotic resonating-valence-bond (RVB) theory of high-Tc superconductivity. Fe-pnictide superconducting materials also crystalize in the layered structure with Fe-As layers separated by alkaline metal ions or other insulator-like layers. Band structure calculations based on the local-density approximation (LDA) or generalized gradient approximations (GGA) indicate dominantly two-dimensional (2D) cylinder-like Fermi surfaces (FSs) along the c-axis.[2–4] It is important to see whether or not the Fe-pnictides share similar anisotropic charge dynamical properties with cuprates.

Optical spectroscopy is a powerful technique to investigate charge dynamics and band structure of a material as it probes both free carriers and interband excitations. In particular, it yields direct information about the energy gap formation in the broken symmetry state. Optical spectroscopy studies on the ab-plane properties of different Fe-pnictides and chalcogenides systems have been reported by several groups.[5–17] For the parent compounds of Fe-pnictides, the measurements provide clear evidence for the formation of the partial energy gaps in the magnetic phase, supporting the itinerant picture that the energy gain for the antiferromagnetic ground state is achieved through the opening of a spin-density-wave (SDW) gap on the FSs.[6, 9, 13–15] For the superconducting samples, the superconducting pairing gaps were also detected by the technique.[5, 16, 17] However, optical investigations have not been carefully done on the c-axis response of Fe-pnictide materials. There is only one work in the literature containing optical data along the c-axis.[9] Unfortunately, the data were limited to the high

frequencies, above 700 cm<sup>-1</sup>. Because of this limitation, neither the free-carrier response nor any feature related to the SDW gap were observed. In fact, the reported reflectance data appear to have extraordinarily low values. As information about the anisotropy of charge dynamics is extremely important for understanding the materials, a detailed and careful determination of the c-axis optical response is highly necessary.

In this letter we present the c-axis ( $\mathbf{E}\parallel\text{c}$ ) optical reflectance measurement over broad frequencies on thick BaFe<sub>2</sub>As<sub>2</sub> single crystal samples. We observed the SDW energy gap formation in the low-T magnetic ordered state. However, different from the ab-plane response where two distinct energy gaps were identified for BaFe<sub>2</sub>As<sub>2</sub>, only the gap corresponding to the smaller energy scale of  $\mathbf{E}\parallel\text{ab-plane}$  could be clearly seen along the c-axis. The more pronounced gap structure at the higher energy scale for  $\mathbf{E}\parallel\text{ab-plane}$  becomes almost invisible. The study also reveals a small anisotropy in the Drude components. The anisotropy ratio of  $\sigma_{1ab}/\sigma_{1c}$  is about 2.8 at 300 K in the low frequency limit, which is further reduced in the low-T magnetic state. A schematic picture for the band structure evolution across the structural/magnetic transition was proposed to understand the experimental findings.

Large-sized single crystals of BaFe<sub>2</sub>As<sub>2</sub> were grown from the FeAs flux in a Al<sub>2</sub>O<sub>3</sub> crucible sealed in a quartz tube. The growth procedure is similar to the description in our earlier work [18] except for one major difference: the crucible and quartz tube were placed in a direction of 45 degree relative to the vertical. After completing the growth procedure and breaking the crucible, we can easily find relatively thick crystals growing from the inner surface of the crucible along the direction at 45 degree relative to the crucible cylinder axis (i.e. crystals grow vertically). A dimension of 5mm×2mm in the ac-plane was selected and finely polished for the c-axis optical measurement. The dc resistivity measured by the four contact technique along the ab-plane was found to be almost identical to the data presented in our early work, showing a sharp drop at 138 K caused by the formation

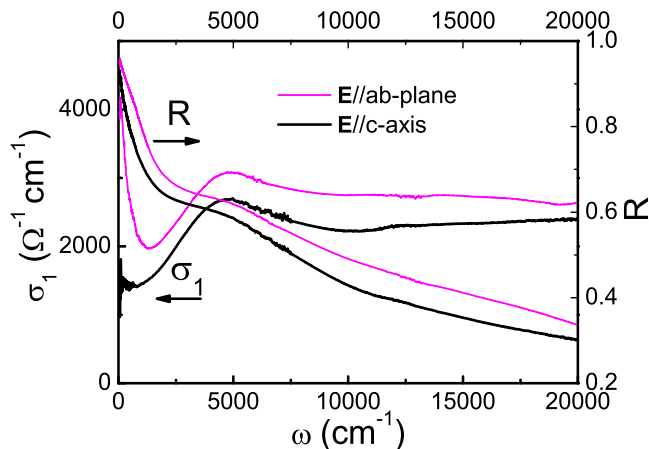


FIG. 1: The c-axis  $R(\omega)$  and  $\sigma_1(\omega)$  at 300 K for  $\text{BaFe}_2\text{As}_2$  over a broad frequency up to  $20000 \text{ cm}^{-1}$ . The ab-plane spectra were also included for a purpose of comparison.[6] The conductivity anisotropy at low frequency limit is about 2.8.

of SDW order.[6] The optical reflectance measurements with  $\mathbf{E}\parallel\text{c-axis}$  were performed on a Bruker IFS 66v/s spectrometer in the frequency range from 50 to  $25000 \text{ cm}^{-1}$ . An *in situ* gold and aluminium overcoating technique was used to get the reflectivity  $R(\omega)$ . The real part of conductivity  $\sigma_1(\omega)$  is obtained by the Kramers-Kronig transformation of  $R(\omega)$ .

Figure 1 shows the c-axis  $R(\omega)$  and  $\sigma_1(\omega)$  at room T over a broad frequency range up to  $20000 \text{ cm}^{-1}$ . For a comparison, we also plot the optical spectra with  $\mathbf{E}\parallel\text{ab-plane}$ [6]. We can see that the overall  $R(\omega)$  along the c-axis is quite similar to that in the ab-plane except for relatively lower values. This is dramatically different from the optical spectra of high-Tc cuprates[1] and other layered compounds, for example, layered ruthenates[19], where the c-axis  $R(\omega)$  shows much lower values and quite different frequency-dependent behavior from the ab-plane. This observation suggests that the band structure of Fe-pnictide should be quite three-dimensional (3D), in contrast to the expectation based on its layered crystal structure. The difference in  $\sigma_1(\omega)$  spectra between ab-plane and the c-axis seems to become larger at low frequencies. An extrapolation to zero frequency, or the dc conductivity, shows an anisotropy ratio of about 2.8. This matches well with the anisotropy ratio determined directly from the dc resistivity measurement by a careful Montgomery technique (about  $3\pm 1$ )[21]. We noticed that the c-axis reflectance values obtained here are much higher than the data presented by Wu et al. on a  $\text{EuFe}_2\text{As}_2$  sample[9]. The reflectance values in their measured frequency range (above  $700 \text{ cm}^{-1}$ ) are already below 0.4, leading to extremely low values of conductivity (below  $100 \text{ }\Omega^{-1}\text{cm}^{-1}$  at  $700 \text{ cm}^{-1}$ ). We remark here that we repeated measurement of  $\mathbf{E}\parallel\text{c}$  on another crystal grown from a different batch and achieved almost iden-

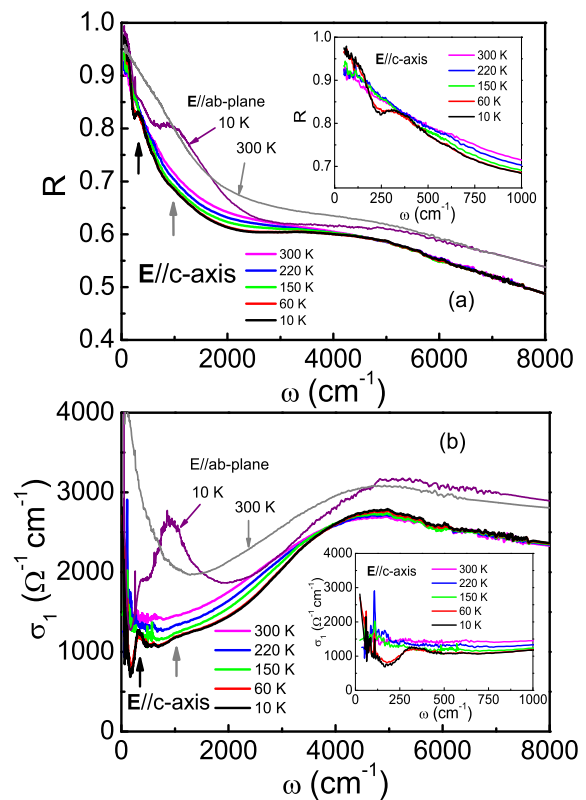


FIG. 2: The c-axis  $R(\omega)$  (a) and  $\sigma_1(\omega)$  (b) at different temperatures below  $8000 \text{ cm}^{-1}$  for  $\text{BaFe}_2\text{As}_2$ . Inset: expanded plot of the low- $\omega$   $R(\omega)$  and  $\sigma_1(\omega)$  spectra. The ab-plane  $R(\omega)$  and  $\sigma_1(\omega)$  at 300 K and 10 K are included for comparison. The two upward arrows indicate the anomalies associated with the SDW order. The very pronounced peak in  $\sigma_1(\omega)$  for  $\mathbf{E}\parallel\text{ab-plane}$  becomes extremely weak for  $\mathbf{E}\parallel\text{c}$ .

tical result.

The temperature dependences of the  $R(\omega)$  and  $\sigma_1(\omega)$  spectra below  $8000 \text{ cm}^{-1}$  ( $\sim 1\text{eV}$ ) are plotted in Fig. 2 (a) and (b), respectively. In the mid-infrared region (near  $4000 \text{ cm}^{-1}$ ), there is a strong suppression feature in both  $R(\omega)$  and  $\sigma_1(\omega)$  spectra. Essentially, the same feature is seen in the ab-plane optical response at slightly higher frequencies (near  $5000 \text{ cm}^{-1}$ ). For a comparison we also plot the in-plane  $R(\omega)$  and  $\sigma_1(\omega)$  spectra at 300 K and 10 K in the figure.[6] The suppression is a common feature for Fe-pnictide materials and is not directly related to the SDW order as it is seen well above the structural/magnetic transition temperature.[6, 12, 15] Its origin remains to be explored. At very low frequencies, the  $R(\omega)$  increases with decreasing T (see inset of Fig. 2(a)), which is consistent with the weak metallic T-dependence of dc resistivity along the c-axis. Again, this is very different from the layered cuprates.[1] Most remarkably, the reflectance is strongly suppressed below  $\sim 320 \text{ cm}^{-1}$  upon entering the SDW ordered state. A sharp upturn appears at lower energy scale. The strong suppression in  $R(\omega)$  re-

sults in a removal of the low- $\omega$  spectral weight in  $\sigma_1(\omega)$  which is transferred to region just above the gap. The sharp upturn at lower frequencies in  $R(\omega)$  leads to a narrow residual Drude component at very low frequencies (see the inset of Fig. 2 (a) and (b)). The data provide clear evidence for the partial energy gap formation along the  $c$ -axis in the SDW ordered phase as well. In the ab-plane optical spectra,[6] we observed two energy gaps in the SDW state with the conductivity peak energies near  $360 \text{ cm}^{-1}$  and  $890 \text{ cm}^{-1}$ . Here we found that the energy scale of the gap  $\mathbf{E}\parallel c$  is close to the smaller one seen in the ab-plane  $\sigma_1(\omega)$ . The more pronounced gap structure at higher energy in  $\mathbf{E}\parallel \text{ab-plane}$  becomes extremely weak in the  $c$ -direction in both  $R(\omega)$  and  $\sigma_1(\omega)$ , as indicated by an upward grey arrow in the figure. The reason will be discussed below.

The optical reflectance measurement down to very low frequencies enables us to analyze the data in a more quantitative way. We are mainly concerned with the evolution of the free carriers. In order to reasonably isolate and estimate the free carrier contributions, we use a Drude+Lorentz model to reproduce  $R(\omega)$  and  $\sigma_1(\omega)$  simultaneously. The dielectric function for a Drude+Lorentz model has the form

$$\epsilon(\omega) = \epsilon_\infty - \frac{\omega_p^2}{\omega^2 + i\omega/\tau} + \sum_{i=1}^N \frac{S_i^2}{\omega_i^2 - \omega^2 - i\omega/\tau_i}. \quad (1)$$

Here,  $\epsilon_\infty$  is the dielectric constant at high energy, the middle and last terms are the Drude and Lorentz components, respectively. With a rough look at the  $R(\omega)$  and  $\sigma_1(\omega)$  in Fig. 1 and 2, one can easily identify a Drude component at low frequency and a pronounced interband transition centered near  $4500 \text{ cm}^{-1}$ . Upon a careful inspection, one can find that the spectral shape near  $1000 \text{ cm}^{-1}$  in  $\sigma_1(\omega)$  (Fig. 2 (b)) could neither be assigned to the Drude component nor ascribed to the tail of the interband transition centered at  $4500 \text{ cm}^{-1}$  since a slope change is seen in the frequency range between  $2000\sim 3000 \text{ cm}^{-1}$ . Therefore, we expect a weak interband transition near  $1000 \text{ cm}^{-1}$ . Now we can use one Drude component and two Lorentz terms (centered near  $4500$  and  $1000 \text{ cm}^{-1}$ ) to fit the high-T far- and mid-infrared reflectance and conductivity data. Below  $T_{SDW}$ , because of partial gap opening, the residual Drude component is pushed to the very low frequencies, a new peak appears near  $320 \text{ cm}^{-1}$ , then we need to add another Lorentz component to reproduce the new SDW gap feature. To reasonably reproduce the high frequency spectra, more Lorentz term(s) have to be included. In fact, we found that with only one extra Lorentz term we can fairly well reproduce  $R(\omega)$  and  $\sigma_1(\omega)$  in the high-T nonmagnetic phase up to  $20000 \text{ cm}^{-1}$ . Nevertheless, we remark that this high-energy Lorentz term has negligible effect on the determination of free carrier parameters.

In Fig. 3 (a) and (b) we show the experimental spectra

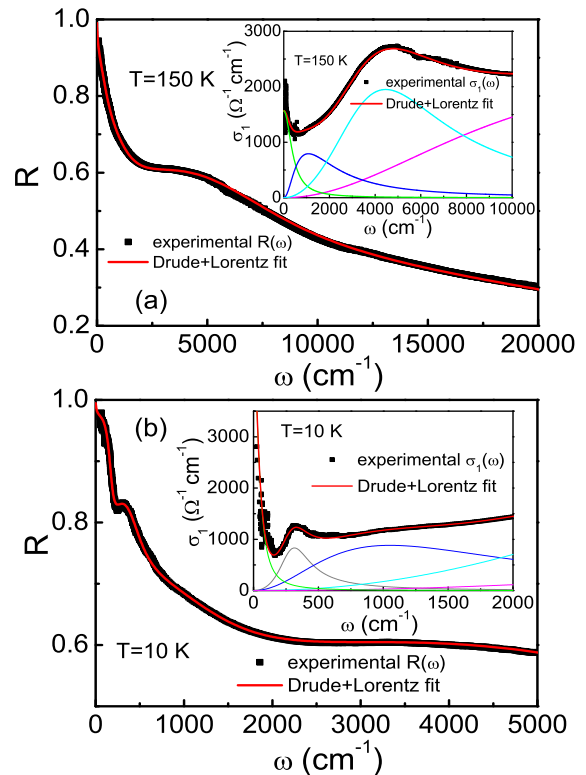


FIG. 3: The experimental  $R(\omega)$  (a) and  $\sigma_1(\omega)$  (b) of  $\text{BaFe}_2\text{As}_2$  for  $\mathbf{E}\parallel c$  and the fitting curves from a Drude+Lorentz model up to different energy scales at 150 K and 10 K, respectively. The same parameters were used to reproduce both  $R(\omega)$  and  $\sigma_1(\omega)$ . The decomposed Drude component and the Lorentz peaks are shown in the inset.

together with fitting curves for two representative temperatures above and below structural/magnetic transition, e.g. at 150 K and 10 K. To show the low-energy feature more clearly in the SDW gapped state, we only plot the curves below  $5000 \text{ cm}^{-1}$  for  $R(\omega)$  and  $2000 \text{ cm}^{-1}$  for  $\sigma_1(\omega)$  at 10 K (Figure 3 (b)). Based on this analysis, we obtained following plasma frequency and scattering rate for the Drude component:  $\omega_p \approx 6300 \text{ cm}^{-1}$  and  $1/\tau \approx 435 \text{ cm}^{-1}$  at 300 K,  $6160 \text{ cm}^{-1}$  and  $405$  at 150 K, and  $3600 \text{ cm}^{-1}$  and  $47 \text{ cm}^{-1}$  at 10 K, respectively. Our earlier study on the ab-plane properties indicates that those two parameters change from  $\omega_p \approx 12900 \text{ cm}^{-1}$  and  $1/\tau \approx 700 \text{ cm}^{-1}$  at 300 K to  $4660 \text{ cm}^{-1}$  and  $55 \text{ cm}^{-1}$  at 10 K.[6]

From those parameters we can see the ratio of  $\omega_p^2(10 \text{ K})/\omega_p^2(150 \text{ K}) \sim 35\%$ . This means that a majority of free carriers (65%) were removed due to the gapping of the FSs associated with SDW order, if we assume that the effective mass of itinerant carriers does not change significantly with T. The removal is smaller along the  $c$ -axis than within ab-plane (which is over 80%)[6, 13]. The anisotropy ratio of the square of plasma frequency  $\omega_{pc}^2/\omega_{pab}^2$  is 24% at 300 K, but increases to 60% at 10 K. This suggests that the SDW order affects the ab-plane

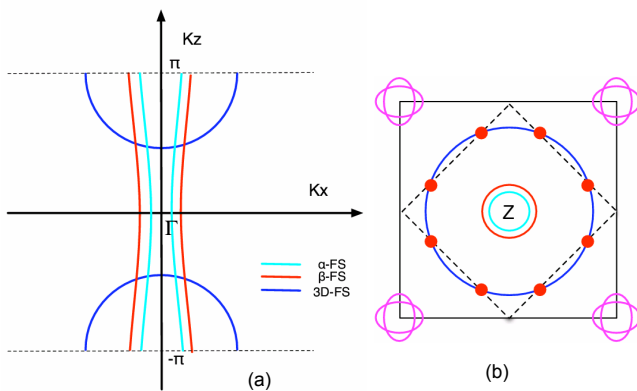


FIG. 4: (a) The schematic plot of the Fermi surfaces along the  $k_z$  direction around the  $\Gamma$  point. Besides the 2D FSs ( $\alpha$  and  $\beta$  bands) there is an additional 3D FS enclosing the Z point  $((0,0,\pi))$ . (b) A top view of the FSs. The magnetic Brillouin zone driven by the  $(\pi, \pi)$  nesting between the disconnected 2D cylinder-like FSs would cut the 3D FS and open gaps in the intersecting points.

more severely than along the  $c$ -axis. The estimation of the data also enables us to calculate the anisotropy of conductivity at zero-frequency limit. Using  $\sigma_{dc} = \omega_p^2 \tau / 4\pi$ , we can get dc conductivity ratio  $\sigma_c / \sigma_{ab} \sim 38\%$  at 10 K, which increases to 69% at 10 K. Here, most of the anisotropy comes from the anisotropy in plasma frequencies. The anisotropy in scattering rate plays a minor role.

Understanding why two distinct gaps could be observed for  $\mathbf{E} \parallel ab$ -plane but only a smaller one could be clearly seen for  $\mathbf{E} \parallel c$ -axis is a crucial issue here. It has important implication for the band structure evolution across the transition. We found that our data could be naturally explained by assuming that there are two types of FSs in the system: the 2D cylinder like FSs and a large-size 3D ellipsoid like FS, as schematically presented in Fig. 4. Presence of the large-size 3D ellipsoid FS with dominant Fe- $3d_{3z^2-r^2}$  orbital is indicated by the recent *ab-initio* LDA+Gutzwiller calculations, where electron correlations are taken into account beyond LDA [20]. Recent transport [21], upper critical field [22], as well as ARPES experiments [23, 24] also suggest the presence of a 3D FS.

If we neglect the small dispersion of those 2D FSs along the  $c$ -axis, the Fermi velocity along the  $c$ -axis becomes zero and the electrons on the 2D FSs would only couple to the polarized light with  $\mathbf{E} \parallel ab$ -plane. On the other hand, the electrons on the 3D FS can couple to the light polarized along any direction. We suggest that the 2D cylinder-like hole FSs around  $\Gamma$  and the 2D electron FSs around M are strongly nested, which is the main driving force for the SDW instability of the system, while the 3D ellipsoid FS does not show any nesting with other FSs. Nevertheless, with the formation of the SDW order driven by the  $(\pi, \pi)$  nesting of 2D FSs, the new mag-

netic Brillouin zone boundary would cut the large-size 3D ellipsoid FS and result in an energy gap at the intersecting points as shown in Fig. 4 (b). This can be seen by optics in both  $\mathbf{E} \parallel ab$ -plane and  $\mathbf{E} \parallel c$ . Then we ascribe the larger gap seen most clearly for  $\mathbf{E} \parallel ab$ -plane to the nesting-driven gap opened on 2D FSs, the smaller one to the gap formed on 3D FS which could be considered as the consequence of the SDW order. Because the 2D FSs are more dramatically affected by the SDW instability than the 3D FS, we expect a reduction of the anisotropy in the magnetic ordered state, which thus is consistent with the experimental observations.

To summarize, we have successfully grown thick single crystals of BaFe<sub>2</sub>As<sub>2</sub> and investigated their optical properties. Our study revealed a clear difference in optical conductivity for  $\mathbf{E} \parallel ab$ -plane and  $\mathbf{E} \parallel c$ -axis in the SDW state. The very pronounced energy gap structure seen at a higher energy scale for  $\mathbf{E} \parallel ab$ -plane is almost invisible for  $\mathbf{E} \parallel c$ -axis, whereas the smaller energy gap could be seen in both polarizations. We propose a novel picture for the band structure evolution and suggest different driving mechanisms for the two energy gaps. The strong  $(\pi, \pi)$  nesting between disconnected 2D cylinder-like FSs is the main driving force for the SDW instability, leading to the opening of larger energy gap in the 2D FSs. The cutting of the magnetic Brillouin zone on the 3D FS leads to a smaller gap at the crossing region. The picture also explains the reduction of the anisotropy in the magnetic ordered state.

This work is supported by the National Science Foundation of China, the Knowledge Innovation Project of the Chinese Academy of Sciences, and the 973 project of the Ministry of Science and Technology of China.

- 
- [1] S. Uchida, K. Tamasaku, and S. Tajima, Phys. Rev. B **53**, 14558 (1996).
  - [2] s. Lebegue, Phys. Rev. B **75**, 035110 (2008).
  - [3] D.J. Singh and M.H. Du, Phys. Rev. Lett. **100**, 237003 (2008).
  - [4] Fengjie Ma and Zhong-Yi Lu, Phys. Rev. B **78**, 033111 (2008).
  - [5] G. Li, W. Z. Hu, J. Dong, Z. Li, P. Zheng, G. F. Chen, J. L. Luo, and N. L. Wang, Phys. Rev. Lett. **101**, 107004 (2008).
  - [6] W. Z. Hu, J. Dong, G. Li, Z. Li, P. Zheng, G. F. Chen, J. L. Luo, and N. L. Wang, Phys. Rev. Lett. **101**, 257005 (2008).
  - [7] F. Pfuner, J. G. Analytis, J.-H. Chu, I. R. Fisher, and L. Degiorgi, Eur. Phys. J. B **67**, 513 (2009).
  - [8] J. Yang, D. Huvonen, U. Nagel, T. Room, N. Ni, P. C. Canfield, S. L. Budko, J. P. Carbotte, and T. Timusk, Phys. Rev. Lett. **102**, 187003 (2008).
  - [9] D. Wu, N. Barišić, N. Drichko, S. Kaiser, A. Faridian, M. Dressel, S. Jiang, Z. Ren, L. J. Li, G. H. Cao, Z. A. Xu, H. S. Jeevan and P. Gegenwart, Phys. Rev. B **79**, 155103 (2009).

- [10] M. M. Qazilbash, J. J. Hamlin, R. E. Baumbach, Lijun Zhang, D. J. Singh, M. B. Maple, D. N. Basov, *Nature Physics* **5**, 647 (2009).
- [11] G. F. Chen, Z. G. Chen, J. Dong, W. Z. Hu, G. Li, X. D. Zhang, P. Zheng, J. L. Luo, N. L. Wang, *Phys. Rev. B* **79**, 140509(R) (2009).
- [12] W. Z. Hu, G. Li, P. Zheng, G. F. Chen, J. L. Luo, N. L. Wang, *Rev. Phys. B* **80**, 100507(R) (2009).
- [13] A. Akrap, J. J. Tu, L. J. Li, G. H. Cao, X. A. Xu, C. C. Homes, *Phys. Rev. B* **80**, 180502(R) (2009).
- [14] S. J. Moon, J. H. Shin, D. Parker, W. S. Choi, I. I. Mazin, Y. S. Lee, J. Y. Kim, N. H. Sung, B. K. Cho, S. H. Khim, J. S. Kim, K. H. Kim, and T. W. Noh, arXiv:0909.3352.
- [15] Z. G. Chen, R. H. Yuan, T. Dong, N. L. Wang, arXiv:0910.1318.
- [16] E. van Heumen, Y. Huang, S. de Jong, A.B. Kuzmenko, M.S. Golden, D. van der Marel, arXiv:0912.0636.
- [17] K. W. Kim, M. Rossle, A. Dubroka, V. K. Malik, T. Wolf, C. Bernhard, arXiv:0912.0140.
- [18] G.F. Chen, Z. Li, J. Dong, G. Li, W.Z. Hu, X.D. Zhang, X.H. Song, P. Zheng, N.L. Wang, and J.L. Luo, *Phys. Rev. B* **78**, 224512 (2008).
- [19] T. Katsufuji, M. Kasai, and Y. Tokura, *Phys. Rev. Lett.* **76**, 126 (1995).
- [20] G. T. Wang, Y. M. Qian, G. Xu, X. Dai, Z. Fang, arXiv:0903.1385 (to be published in *Phys. Rev. Lett.*).
- [21] M. A. Tanatar, N. Ni, G. D. Samolyuk, S. L. Bud'ko, P. C. Canfield, R. Prozorov, *Phys. Rev. B* **79**, 134528 (2009).
- [22] H. Q. Yuan, J. Singleton, F. F. Balakirev, S. A. Baily, G. F. Chen, J. L. Luo, N. L. Wang, *Nature* **457**, 565 (2009).
- [23] C. Liu, G. D. Samolyuk, Y. Lee, N. Ni, T. Kondo, A. F. Santander-Syro, S. L. Bud'ko, J. L. McChesney, E. Rotenberg, T. Valla, A. V. Fedorov, P. C. Canfield, B. N. Harmon, A. Kaminski, *Phys. Rev. Lett.* **101**, 177005 (2008).
- [24] W. Malaeb, T. Yoshida, A. Fujimori, M.o Kubota, K. Ono, K. Kihou, P. M. Shirage, H. Kito, A. Iyo, H. Eisaki, Y. Nakajima, T. Tamegai, R. Arita, *J. Phys. Soc. Jpn.* **78**, 123706 (2009).